Microscopic spin interactions in colossal magnetoresistance manganites

J. A. Fernandez-Baca,[1] Pengcheng Dai,[2,1] H. Kawano-Furukawa,[3] H. Yoshizawa,[4] E. W. Plummer,[2,1] S. Katano,[5] Y. Tomioka,[6,7] and Y. Tokura[6,7,8]

[1]*Solid State Division, Oak Ridge National Laboratory, Oak Ridge, Tennessee 37831-6393*

[2]*Department of Physics and Astronomy, University of Tennessee, Knoxville, Tennessee 37996-1200*

[3]*Department of Physics, Faculty of Science, Ochanomizu University Otsuka 2-1-1, Bunkyo-ku, Tokyo 112-8610, Japan*

[4]*Neutron Scattering Laboratory, Institute for Solid State Physics, University of Tokyo, Shirakata 106-1, Tokai, Ibaraki 319-1106, Japan*

[5]*Advanced Science Research Center, Japan Atomic Energy Research Institute (JAERI), Tokai, Ibaraki 319-1195, Japan*

[6]*Joint Research Center for Atom Technology (JRCAT), Tsukuba 305-0046, Japan*

[7]*Correlated Electron Research Center (CERC), Tsukuba 305-8562, Japan*

[8]*Department of Applied Physics, University of Tokyo, Tokyo 113-8656, Japan*

(Received 4 June 2002; published 26 August 2002)

Using inelastic neutron scattering we measured the microscopic magnetic coupling associated with the ferromagnetic clusters of the ''colossal magnetoresistance'' compound $Pr_{0.70}Ca_{0.30}MnO_3$. When the insulating-to-metal (I-M) transition is induced by an external magnetic field there is a discontinuous change in the spin-wave stiffness constant. This result implies that the I-M transition is not achieved by the simple percolation of micron-sized metallic clusters as currently believed, but involves a first-order transformation.

DOI: 10.1103/PhysRevB.66.054434 PACS number(s): 72.15.Gd, 61.12.Ld, 71.30.+h

The understanding of the colossal magnetoresistance (CMR) effect—the unusually large change in electrical resistance in response to a magnetic field—in certain materials is among the most interesting unresolved problems in condensed matter physics.[1] The most studied of these materials are the doped perovskite manganites $A_{1-x}B_xMnO_3$ [where A is a trivalent ion (La^{3+}, Pr^{3+}, Nd^{3+}, etc.) and B is a divalent ion (Ca^{2+} or Sr^{2+})] with $x \approx 0.3$. The basic microscopic mechanism responsible for the CMR effect is believed to be the double-exchange (DE) interaction,[2] where ferromagnetism and electrical conductivity arise from hopping of the itinerant e_g electrons from trivalent Mn^{3+} to tetravalent Mn^{4+} sites. The physics of the CMR effect, however, is far from being completely understood. Recent calculations suggest that these materials are intrinsically inhomogeneous and have a strong tendency to spatial electronic phase separation,[3] and electron microscopy and tunneling experiments suggest that the insulating-to-metal (I-M) transition is achieved via the percolation of large (micron-size) metallic clusters.[4,5] While this mesoscopic percolation scenario is attracting considerable attention, such a picture is difficult to reconcile with experiments that indicate that the I-M transition involves a first-order transformation, a large release of energy, and a strong irreversibility.[6] In this paper, we show that the I-M transition in $Pr_{0.70}Ca_{0.30}MnO_3$ (PCMO30) is indeed far more complex than the simple percolation of micron-sized metallic clusters. Instead, our study of PCMO30 shows that this transition is associated with insulating ferromagnetic (FM) regions that become metallic in a first-order process. This result challenges our present understanding of the CMR effect and suggests that, if percolation plays an important role in the CMR process, it must be the percolation of insulating clusters in conjunction with an underlying first-order phase transition.

PCMO30 is an ideal system to test the mesoscopic phase separation scenario, because it has an inhomogeneous low-temperature insulating state[7–9] where ferromagnetism, antiferromagnetism, and charge ordering coexist.[10] This insulating state is metastable and can be converted to a metallic state by the application of an external magnetic[10,11] or electric field,[12] high pressure,[13] and exposure to x rays[14] or visible light.[15] In the mesoscopic electronic phase separation picture,[4,5] the electrical conductivity in the CMR materials is achieved via the percolative transport of carriers through micrometer-sized FM metallic domains in an insulating antiferromagnetic (AF) background. In this scenario the effect of an external magnetic field would be only to enlarge the FM metallic clusters, at the expense of the AF insulating regions, without modifying the magnetic coupling of the spins. We use inelastic neutron scattering to probe the microscopic magnetic coupling associated with the FM clusters in PCMO30. We achieve this by measuring the FM spin-wave (SW) stiffness constant D (which measures the strength of the magnetic coupling of the spins[16]) as PCMO30 undergoes the I-M transition induced by a magnetic field. The use of thermal neutrons, which probe length scales of the order of a few hundred angstrom, ensures that our measurements are insensitive to FM cluster-size changes at micron scales. For a conventional ferromagnet the effect of an external magnetic field of a few tesla is limited to induce a small Zeeman gap in the SW dispersion relation, with no change in D.[18] Surprisingly, when the I-M transition in PCMO30 is induced by a 3.5 T field at low temperature there is also a threefold discontinuous change in the magnitude of D. This unexpected result indicates that the I-M transition involves a first-order transformation from insulating to metallic clusters, and not just the simple percolation of large metallic clusters as proposed in the mesoscopic percolation picture. Thus, any realistic percolation model of the I-M transition must account for the microscopic interactions of the spins and the first-order nature of the I-M transition.

For this study, we prepared a single crystal of PCMO30 by the floating-zone method.[11] Transport and electron-probe microanalysis on different parts of the crystal indicated that

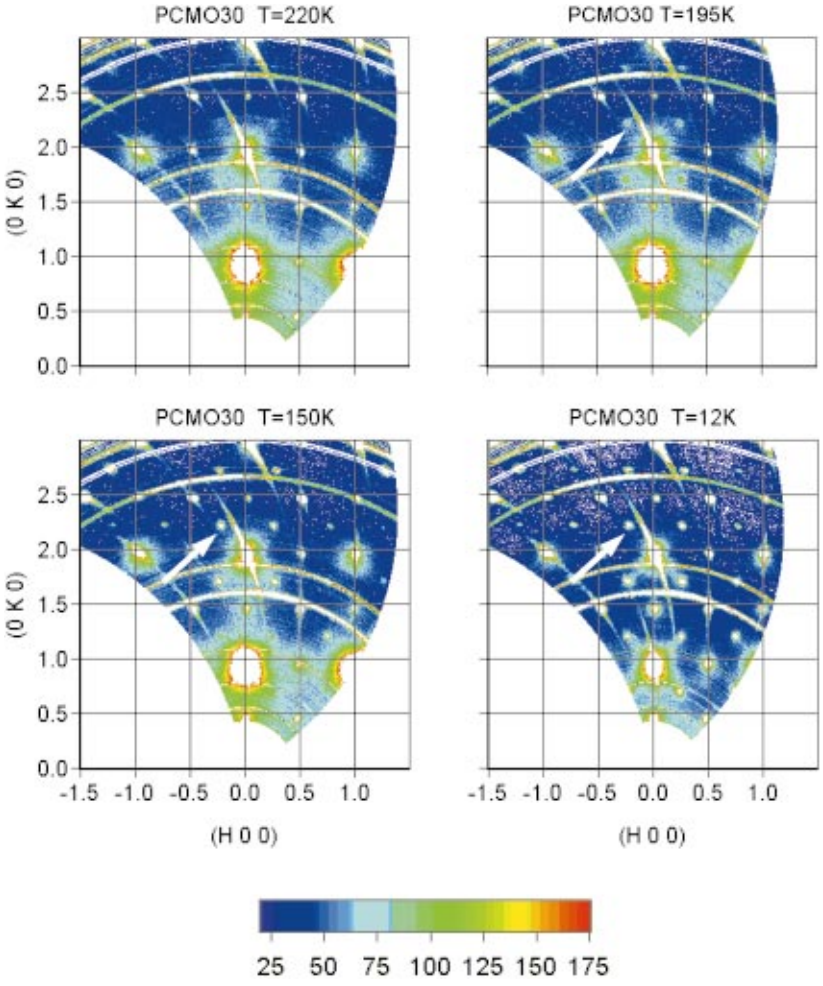

FIG. 1. (Color) Neutron diffraction patterns of PCMO30 in the $(H,K,0)$ reciprocal lattice plane (pseudocubic notation). The white arrows indicate the region near the $(\pm\delta,2\pm\delta,0)$ $(\delta=1/4)$ satellites expected for the CE-type charge ordering. The rings around the origin correspond to scattering from the aluminum sample holder, and the narrow ''streaks'' through the strong Bragg peaks are an artifact of the detector.

the Ca doping was homogeneous. The crystal has a mosaic spread of about 1° degree and a volume of 0.4 cm^3. The neutron scattering measurements were performed at Oak Ridge National Laboratory's High Flux Isotope Reactor. Most of the measurements were performed using triple-axis spectrometers configured to provide an energy resolution at the elastic $(E=0)$ position of $\Delta E=0.55$ meV [full width at half maximum (FWHM)].[19] Neutron diffraction measurements were also carried out at the Wide Angle Neutron Diffractometer (WAND).[20,21]

PCMO30 has an orthorhombic structure slightly distorted from the cubic lattice. For simplicity, we label the wave vectors $Q=(q_x,q_y,q_z)$ in units of $Å^{-1}$ as $(H,K,L)=(q_xa/2\pi,q_ya/2\pi,q_za/2\pi)$ in the reciprocal lattice units (rlu) appropriate for the pseudocubic unit cells with lattice parameter $a\approx3.87$ Å. In this convention all (H,K,L) $(H,K,L$ integers) reflections are allowed. The crystal was oriented to allow wave vectors of the form $(H,K,0)$ to be accessible in the scattering plane. PCMO30 has a complex sequence of transitions.[10] Below $T_{CO}\approx200$ K it exhibits charge ordering while remaining paramagnetic and below $T_N\approx140$ K the magnetic moments associated with the Mn^{3+} and Mn^{4+} ions order antiferromagnetically in the so-called pseudo CE-type structure. It is only below $T_C\approx110$ K that the system develops a FM component that coexists with the CE-type antiferromagnetism. At zero magnetic field PCMO30 remains an insulator at all temperatures. The charge-ordered and antiferromagnetic phases are both characterized by satellite reflections $(1/4,1/4,0)$ and $(1/2,0,0)$ (and equivalent reflections).

We collected data under two different conditions, first by applying a magnetic field after the sample was cooled in zero field [zero-field cooling (ZFC)] and by cooling the sample under an applied field (field cooling or FC). The magnetic field was applied perpendicular to the scattering plane by an Oxford cryomagnet $(0\ \text{T}\leqslant H\leqslant7.0\ \text{T})$. The ZFC with $H=0$ measurements revealed the clear presence of diffuse scattering around the main Bragg peaks above T_C (see Fig. 1). This diffusive component is strongest at the smaller wave vectors and becomes gradually weaker as the wave vector increases, as expected for the magnetic form factor of the Mn ions, indicating that this scattering is magnetic. When the sample is cooled below T_C a long-range FM component[17] develops [additional Bragg intensity at the (H,K,L) positions], at the same time that the diffuse scattering becomes weaker. This diffusive component, however, does not vanish even at the lowest temperatures, indicating the inhomogeneous character of this system at zero field. In addition to the diffuse scattering there are additional superlattice reflections indicating the antiferromagnetism associated with the charge ordering of the pseudo CE type. This ordering has characteristic wave vectors $(\pm1/4,\pm1/4,0)$ (see Fig. 1). From the

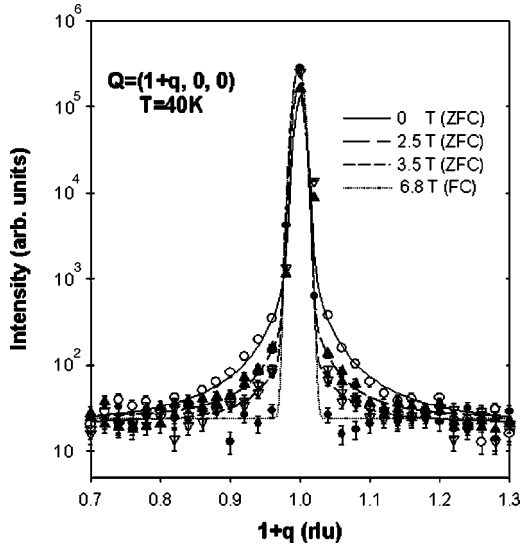

FIG. 2. $Q=(1+q,0,0)$ scattering profiles for $H=0$, 2.5, and 3.5 T (ZFC) and 6.8 T (FC). The solid lines are the results of least-squares fits to Lorentzian (diffuse) and Gaussian (Bragg) components, except for the FC data which have only a Gaussian component.

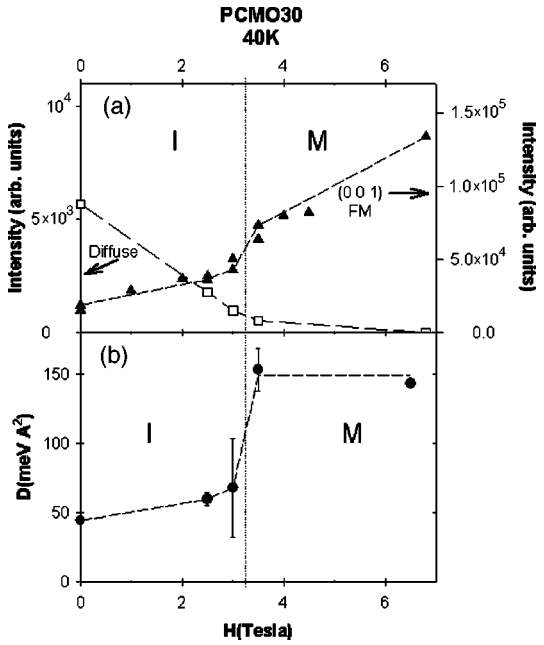

FIG. 3. (a) ZFC magnetic field dependence of the intensities of the Bragg (solid triangles) and Lorentzian (open squares) components of the (1,0,0) FM reflection. The dashed lines are a guide to the eye. The dotted line at $H\approx 3.5$ T indicates the I-M boundary. (b) ZFC magnetic field dependence of the low-q SW stiffness coefficient D at $T=40$ K.

sharpness of the charge ordering peaks, it is clear that the charge ordering in PCMO30 is long range[17] in contrast to the short-range charge ordering in $La_{1-x}Ca_xMnO_3$ family of materials.[22,23]

Figure 2 shows the ZFC elastic scattering profiles of the (100) Bragg peak at $T=40$ K measured with a triple-axis spectrometer, for $H=0$, 2.5, and 3.5 T. The long-range Bragg component[17] of the scattering has been fitted to a Gaussian while the magnetic diffusive component has been fitted to a Lorentzian line shape. The magnetic diffuse scattering indicates the presence of short-range FM clusters with a correlation length $\xi\approx 40$ Å. These nano-size clusters are static within a $\Delta t\approx 1$ ps and coexist with ''large'' [long-range FM (Ref. 17)] clusters. The effect of the magnetic field is to gradually reduce the number of the nano-size clusters, without significantly changing their correlation length, at the same time that the ferromagnetic moment is increased. This is reflected by the intensity reduction of the Lorentzian component without a significant change in its linewidth, while the intensity of the Bragg component increases (Fig. 2). When the system is FC at 6.8 T, there is no trace of the Lorentzian component. The (ZFC) magnetic field dependence of the intensities of these two components has been plotted in Fig. 3(a). The region where there is a jump in the intensity of the FM component (around 3.5 T) corresponds to the I-M transition, which is also the region where the CE-type antiferromagnetism is greatly (but not completely) suppressed.[10]

We also measured the spin waves in PCMO30 both in the FC and ZFC conditions. First we measured the spin waves at 40 K after the sample was cooled in a 6.8-T field. Then the field was gradually decreased to 5 T, 2 T, and 0.5 T and the low-q ($q\leqslant 0.07$ rlu) spin waves were measured for every field. The measurements were made in the constant $Q=(1+q,0,0)$ mode. The SW energies followed the usual quadratic dependence expected for a ferromagnet in the long-wavelength (small q) limit: $E(q)=\Delta+Dq^2$, where Δ is the Zeeman energy gap and D is the SW stiffness coefficient.[18] This is shown in Fig. 4(a), where the measured FC low-q SW energies have been plotted vs q^2 for various magnetic fields; the straight lines are the result of fits to the quadratic dispersion relation. The upper inset of Fig. 4(a) shows a plot of the fitted SW stiffness coefficient D vs H. Within the experimental error the SW stiffness does not change with the field (after FC at 6.8 T) and has a value of $D=(140\pm 5)$ meV Å^2 at $T=40$ K. Thus, the only effect of the field in the FC case is to open a Zeeman energy gap that grows linearly with the applied field as $\Delta=g\mu H$ [see lower inset of Fig. 4(a)], where μ is the FM moment that contributes to the spin-wave measurements. We note that the magnetic moment obtained from this plot is only $\mu=(2.57\pm 0.43)\mu_B$, which is smaller than the expected full Mn moment of $3.7\mu_B$ for the $x=0.30$ doped Mn^{3+}/Mn^{4+} system. This reduced value of μ may indicate that the FM moments may be canted as originally proposed by Yoshizawa *et al.*[10]

The low-q SW excitations at $T=40$ K in the ZFC condition were different. Unlike the FC case, the ZFC measurements had to be performed in the constant-E mode due to the high background related to the strong FM diffusive component mentioned above, which is strongest in the vicinity of $Q=(1,0,0)$. In all cases the SW energies also followed the expected quadratic dependence; the results from these measurements have been plotted in Fig. 4(b). The surprising result is that the ZFC SW stiffness coefficient for fields up to ≈ 3 T is only $D\approx 50$ meV Å^2, almost a factor of 3 smaller than for the FC case. The full stiffness $D=(140$

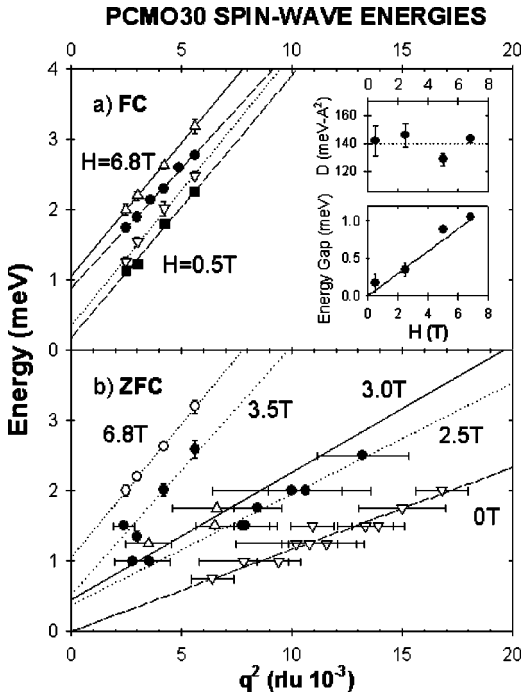

FIG. 4. (a) FC low-q SW energies vs q^2 showing the usual quadratic dispersion $E=\Delta+Dq^2$ expected for a FM. Upper inset: FC SW stiffness coefficient vs H. Lower inset: fitted energy gap Δ vs magnetic field showing the expected linear Zeeman relation. (b) ZFC low-q SW energies vs q^2 showing the usual quadratic dispersion $E=\Delta+Dq^2$ expected for a FM. Note the drastic change in the slope (D coefficient) at $H\approx 3.5$ T, when the I-M transition occurs.

$\pm 5)$ meV Å^2 is only recovered when the I-M transition is induced at $H\approx 3.5$ T [see Fig. 3(b)], at the same time when the $\xi\approx 40$ Å clusters are suppressed.

The sharp threefold change in D suggests either a drastic change in the magnitude of the spins or a drastic change in the strength of the spin interactions at the PCMO30 field-induced I-M transition. The first possibility can be ruled out from Fig. 3(a) as the magnitude of the small change in the FM component cannot account for the magnitude of the observed change in D. Our findings thus favor a drastic change in the strength of the microscopic spin interactions at the I-M transition. We note that the high SW stiffness $D=(140 \pm 5)$ mev Å^2 is comparable to that of other FM metallic manganites near the $x=0.30$ doping,[24] where double exchange seems to be the dominant magnetic interaction. It is tempting to attribute the low SW stiffness $D\approx 50$ meV Å^2 to the effect of the nano-size clusters (short-range FM clusters mentioned above) observed in the insulating phase, the idea being that the propagation of spin waves in these small clusters could be—in principle—different to that in the larger (hundreds of angstroms) clusters. We note, however, that the low SW stiffness $D\approx 50$ meV Å^2 is similar to that of the recently measured FM insulator $La_{0.80}Ca_{0.20}MnO_3$,[25–27] and it is likely that the observed low SW stiffness D is associated with ''large'' (long-range FM regions[17]) insulating clusters. It is not clear if the nano-size (short-range FM) regions would support the propagation of spin waves, but if they do, it is likely that they would be affected by severe lifetime effects and strong damping. These strongly damped excitations could be a source of the high background observed in these measurements.

Thus in our picture the insulating region is composed of large (i.e., greater than a few hundred angstroms) FM insulating clusters and of FM nano-sized clusters. The application of an external magnetic field reduces the number of the nano-size clusters until the system becomes metallic in a first-order transition. This is consistent with two recent reports of thermodynamic measurements in PCMO30. Roy *et al.*[6] reported an enormous release of energy and a strong irreversibility at the I-M transition of this system. Deac *et al.*[28] suggested the existence of field-induced insulating clusters in this material at low magnetic fields. Our results are inconsistent with the mesoscopic phase separation picture,[4,5] in which the I-M transition in the CMR materials is associated with the percolation of micron-size FM metallic domains (if these were the case, these regions would exhibit the high SW stiffness $D=(140\pm 5)$ mev Å^2 even in the insulating phase), and that the physics involved in the I-M transition is far more complex. One possible scenario of the I-M transition in the CMR materials could involve the percolation of insulating clusters in conjuction with an underlying first-order transition. It is known that random quenched disorder may or may not produce rounding of a first-order phase transition. This was first studied by Imry and Wortis[29] and more recently by Moreo *et al.*[30] This is a challenge to the current theoretical approaches of CMR.

Finally, we note that the nano-size FM clusters of Fig. 2 are comparable in size to those observed in other CMR materials above and at their FM transition temperatures.[24,31,32] The field dependence of the nano-size FM clusters of Fig. 3(a) seems to imply that these nano-size clusters do play some role in the I-M transition.

This work was supported by the U.S. DOE under Contract No. DE-AC05-00OR22725 with UT-Battelle, LLC, by NSF Grant No. DMR-0139882, and by JRCAT and CERC of Japan. This work was performed under the U.S.-Japan Cooperative Program on Neutron Scattering. We acknowledge helpful discussions with R. Fishman, E. Dagotto, S-W. Cheong, and N. Furukawa and the expert technical support provided to us by R. G. Maples, S. Moore, and G. B. Taylor.

[1] Masatoshi Imada, Atsushi Fujimori, and Yoshinori Tokura, Rev. Mod. Phys. **70**, 1039 (1998).
[2] C. Zener, Phys. Rev. **82**, 403 (1951).
[3] E. Dagotto, T. Hotta, and A. Moreo, Phys. Rep. **344**, 1 (2001).
[4] M. Uehara, S. Mori, C.H. Chen, and S-W. Cheong, Nature (London) **399**, 560 (1999).
[5] M. Fäth, S. Freisem, A.A. Menovsky, Y. Tomioka, J. Aarts, and J.A. Mydosh, Science **285**, 1540 (1999).

[6] M. Roy, J.F. Mitchell, A.P. Ramirez, and P. Schiffer, Phys. Rev. B **62**, 13876 (2000).
[7] D.E. Cox, P.G. Radaelli, M. Marezio, and S-W. Cheong, Phys. Rev. B **57**, 3305 (1998).
[8] P.G. Radaelli, R.M. Ibberson, S-W. Cheong, and J.F. Mitchell, Physica B **276**, 551 (2000); P.G. Radaelli, R.M. Ibberson, D.N. Argyriou, H. Casalta, K.H. Andersen, S-W. Cheong, and J.F. Mitchell, Phys. Rev. B **63**, 172419 (2001).
[9] C. Frontera, J.L. Garca-Muoz, A. Llobet, M. Respaud, J.M. Broto, J.S. Lord, and A. Planes, Phys. Rev. B **62**, 3381 (2000).
[10] H. Yoshizawa, H. Kawano, Y. Tomioka, and Y. Tokura, Phys. Rev. B **52**, R13 145 (1995); J. Phys. Soc. Jpn. **65**, 1043 (1996).
[11] Y. Tomioka, A. Asamitsu, H. Kuwahara, Y. Moritomo, and Y. Tokura, Phys. Rev. B **53**, R1689 (1996).
[12] A. Asamitsu, Y. Tomioka, H. Kuwahara, and Y. Tokura, Nature (London) **388**, 50 (1997).
[13] Y. Moritomo, H. Kuwahara, Y. Tomioka, and Y. Tokura, Phys. Rev. B **55**, 7549 (1997).
[14] V. Kiryukhin, D. Casa D, J.P. Hill, B. Keimer, A. Vigliante, Y. Tomioka, Y. Tokura, Nature (London) **386**, 813 (1997).
[15] K. Miyano, T. Tanaka, Y. Tomioka, and Y. Tokura, Phys. Rev. Lett. **78**, 4257 (1997).
[16] The SW stiffness constant D is proportional to magnetic exchange constant J in the Heisenberg ferromagnet model and to the kinetic energy term in the DE model.
[17] Within our probe ''long-range'' means greater than a few hundred angstroms.
[18] S. Lovesey, *Theory of Thermal Neutron Scattering from Condensed Matter* (Clarendon, Oxford, 1984), Vol. 2, Chap. 9.
[19] This was obtained using pyrolytic graphite (PG) as monochromator [PG(0 0 2)] and filters and a beryllium analyzer [Be(1 0 1)]. The final neutron energy was fixed at $E_f = 13.6$ meV with collimations of, proceeding from the reactor to the detector, 40-20-40-120 min (FWHM).
[20] The WAND is a flat-cone geometry diffractometer built by JAERI and ORNL as part of the U.S.-Japan Cooperative Program on Neutron Scattering.
[21] S. Katano, J.A. Fernandez-Baca, and Y. Yamada, Physica B **214-243**, 198 (1998).
[22] Pengcheng Dai, J.A. Fernandez-Baca, N. Wakabayashi, E.W. Plummer, Y. Tomioka, and Y. Tokura, Phys. Rev. Lett. **85**, 2553 (2000).
[23] C.P. Adams, J.W. Lynn, Y.M. Mukovskii, A.A. Arsenov, and D.A. Shulyatev, Phys. Rev. Lett. **85**, 3954 (2000).
[24] J.A. Fernandez-Baca, P. Dai, H.Y. Hwang, C. Kloc, and S-W. Cheong, Phys. Rev. Lett. **80**, 4012 (1998) .
[25] G. Biotteau, M. Hennion, F. Moussa, J. Rodrguez-Carvajal, L. Pinsard, A. Revcolevschi, Y.M. Mukovskii, and D. Shulyatev, Phys. Rev. B **64**, 104421 (2001).
[26] Pengcheng Dai, J.A. Fernandez-Baca, E.W. Plummer, Y. Tomioka, and Y. Tokura, Phys. Rev. B **64**, 224429 (2001).
[27] T. Okuda, Y. Tomioka, A. Asamitsu, and Y. Tokura, Phys. Rev. B **61**, 8009 (2000).
[28] I.G. Deac, J.F. Mitchell, and P. Schiffer, Phys. Rev. B **63**, 172408 (2001).
[29] Y. Imry and M. Wortis, Phys. Rev. B **19**, 3580 (1979).
[30] Adriana Moreo, Matthias Mayr, Adrian Feiguin, Seiji Yunoki, and Elbio Dagotto, Phys. Rev. Lett. **84**, 5568 (2000).
[31] J.W. Lynn, R.W. Erwin, J.A. Borchers, Q. Huang, A. Santoro, J-L. Peng, and Z.Y. Li, Phys. Rev. Lett. **76**, 4046 (1996).
[32] J.M. de Teresa *et al.*, Nature (London) **386**, 257 (1997).